Cable deformation simulation and a hierarchical framework for Nb_3Sn Rutherford cables

D Arbelaez, S O Prestemon, P Ferracin, A Godeke, D R Dietderich and G Sabbi

Lawrence Berkeley National Laboratory, Berkeley, CA 94720, USA

E-mail: darbelaez@lbl.gov

Abstract. Knowledge of the three-dimensional strain state induced in the superconducting filaments due to loads on Rutherford cables is essential to analyze the performance of Nb_3Sn magnets. Due to the large range of length scales involved, we develop a hierarchical computational scheme that includes models at both the cable and strand levels. At the Rutherford cable level, where the strands are treated as a homogeneous medium, a three-dimensional computational model is developed to determine the deformed shape of the cable that can subsequently be used to determine the strain state under specified loading conditions, which may be of thermal, magnetic, and mechanical origins. The results can then be transferred to the model at the strand/macro-filament level for rod restack process (RRP) strands, where the geometric details of the strand are included. This hierarchical scheme can be used to estimate the three-dimensional strain state in the conductor as well as to determine the effective properties of the strands and cables from the properties of individual components. Examples of the modeling results obtained for the orthotropic mechanical properties of the Rutherford cables are presented.

1. Introduction

The ability to obtain the three dimensional strain state in Nb_3Sn filaments is of key importance in understanding the performance of Nb_3Sn magnets under macro-scale loads. However, this is a difficult task due to the widely varying length scales in superconducting magnets. For example, some of the length scales that play an important role are the magnet, coil, cable, strand, and filament length scales, where the magnet and coil are in the m scale, the cable and strand in the mm scale, and the filaments in the μm scale. Clearly, the direct simulation of the macro-scale problem including the micro-scale details is prohibitably expensive; therefore, multi-scale tools that can be used to understand the behavior across various length scales are necessary. The development of such tools could be a significant aid in the understanding of magnet performance and for magnet design. At Lawrence Berkeley National Laboratory (LBNL) work has begun on bridging the full range of scales seen in large accelerator magnets, with specific emphasis on magnets fabricated with Rutherford cables. Since the length scales vary widely, several models, which include the relevant physics at the different length scales, must be created, and efficient techniques must be developed to bridge these scales. In this paper the main focus, within this larger framework, is on the development of models at the cable and strand scale that bridge the behavior between the coil scale and the length scale of a macro-filament in a rod restack process (RRP) strand.

Computational models that are used to determine the strain state in Nb_3Sn filaments have been developed by several researchers. For example, Mitchell [1, 2] developed one and two-dimensional models to determine the strain state inside the Nb_3Sn filaments from thermo-mechanical loads on a strand. The one-dimensional model considers the different materials in the strand by their cross-sectional area fraction and includes plastic deformation which is shown to play a critical role. Ahoranta and collaborators [3] developed a two-dimensional model for Nb_3Sn strands where in only certain parts of the strand the geometry are considered in full detail (including filaments), while the rest of the strand is modeled with a simplified geometry. Boso and collaborators [4, 5] developed a hierarchical multi-scale procedure to model Nb_3Sn conductors. For the deformation of subelements during the cabling procedure, Farinon and collaborators [6, 7] developed a model to determine the deformation of powder in tube (PIT) and internal tin (IT) strands in a two-dimensional setting.

In this work, a computational model that is used to determine the three-dimensional deformation of a Rutherford cable during a cabling process will be presented. In this model, a regular unaligned mesh is used and the strand material is treated as a homogeneous elasto-plastic solid. In order to simplify the analysis, the void space between the strands is meshed and treated with a fictitious material. The properties of this fictitious material are chosen such that it can undergo large deformations, while transferring a negligible amount of load to the strand material, until it becomes highly compacted. At this point, the material stiffens considerably and transfers the contact load between strands or between a strand and the boundary. Using the deformed shape, a coil unit cell is created which includes the deformed cable, an insulation layer, and the interstitial epoxy. The effective (homogenized) properties of the coil are then computed using a homogenization scheme. The model presented in this work allows for calculations across three scales. The loads from the analysis of a coil in a magnet can be applied to the cable/insulation unit cell, and the loads at a region in the cable can be applied to a RRP macro-filament unit cell. The strain state in the RRP macro-filaments are considered only for the linear elastic case. For this model the loads can be transferred directly from the cable model to the macro-filament unit cell model since there are only a few macro-filaments from the center to the edge for the strands which are currently used at LBNL; therefore, the length scale for this unit cell can be considered to be close to being on the same order of magnitude as the length scale for the strand. In this work, the simulation of the cable deformation to obtain the initial geometry and a simplified hierarchical framework (including only linear elastic behavior) for Nb_3Sn Rutherford cables are presented.

2. Rutherford cable model

In this section a simulation of the cabling process is presented and a procedure to determine the effective properties of a coil is demonstrated using the final deformed shape of the cable. Results for several test cases are also presented.

2.1. Initial Rutherford Cable Geometry

The first task in determining the shape of the Rutherford cable is to obtain the initial cable geometry. This geometry is never really constructed in a real cabling process, but it serves as a starting point for these simulations. This initial configuration corresponds to an undeformed Rutherford cable where the cross-sections of the strands remain cylindrical. The geometry of the cable in its initial state is defined by three parameters: the number of strands N, the diameter of the strands d, and the initial pitch angle ϕ_0. By using the cable symmetry, the length of the cable section that is modeled is set by the smallest possible repeating unit cell, which corresponds to the axial distance over which a strand cross-section translates one unit. This distance can be

expressed as

$$l_u = \frac{d}{\sin \phi_0}, \tag{1}$$

where d is the strand diameter and ϕ_0 is the pitch angle of the undeformed cable. The creation of the inner strands is trivial since they are simply cylinders rotated about the axial direction of the cable by the angle ϕ_0; however, the edge strand has more strict requirements. Without loss of generality, an edge strand can be considered that starts on the top with pitch angle ϕ_0 and exits at the bottom with pitch angle $-\phi_0$. The requirements for this strand are that its axis must form an angle ϕ_0 with the cable axis at $z = 0$, must form an angle $-\phi_0$ with the cable axis at $z = l_u$, and a must have an elevation angle of zero at both of these points. The edge strand is also required to remain in contact with at least one of the two neighboring strands throughout the unit cell length. One possible solution for the curve that defines the axis of the strand is the intersection of two cylinders each with diameter $2d$ that are offset in the vertical direction by a distance d and have angles of ϕ_0 and $-\phi_0$ respectively (see figure 1). This solution meets all of the restrictions and is chosen for our simulations; however, it is not expected to be the only possible solution for the previously identified constraints. For the initial configuration, this intersection is solved numerically and the curve that defines the axis is discretized in a piecewise manner. Figure 2 shows the initial undeformed cable geometry.

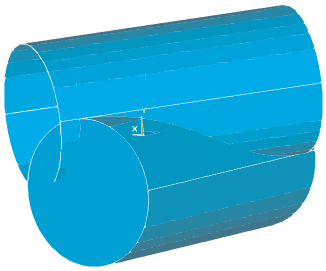

Figure 1. The intersection between these two cylinders is taken as the axis of the end strand in the initial configurations of the Rutherford cable model.

2.2. Material models and mesh generation

In the cable deformation model, an unaligned regular mesh is used along with an elasto-plastic strand material and a fictitious void material. This approach is chosen since it circumvents the need to generate a complicated mesh and does not require contact elements. The contact

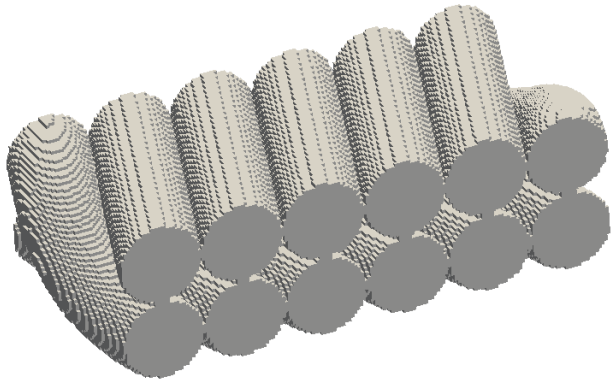

Figure 2. Initial undeformed cable configuration used for the cable deformation simulation.

is simulated by the stiffening of the fictitious void material as it becomes highly compressed. For the meshing procedure, a regular mesh is generated on a rectangular block with eight-node hexahedral "brick" elements. Each element can then be composed of different materials. For the large deformation cabling simulations three different types of elements are considered: elements that contain only the strand material, elements that contain only the fictitious void material, and interface elements which contain both materials. Initially, the interface materials are treated as the void material if the total volume of the element exceeds the volume of strand material inside that element. Once the total volume of the element falls below the volume of strand material inside the element, that element is converted to an elasto-plastic strand element. Hyper-elastic constitutive models are used for both the elastic part of the strand deformation and for the fictitious void material. For the strand, a large deformation elasto-plastic model by Simo [8] is used. This model uses the von Mises yield criterion and an associated flow rule. In this work an isotropic hardening law is used and the functional form is chosen to be a power law, which is given by

$$k = A\varepsilon^n, \tag{2}$$

where A and n are determined by using data for the Young's modulus, the proportional limit, the ultimate tensile strength, and the elongation to failure. For the simulations presented in this work, data for copper is used, which is shown in table 1.

The fictitious void material is modeled with a hyper-elastic law that is modified so that it is highly compressible, but also becomes infinitely stiff as the volume at a point vanishes. For Hyper-elastic materials a strain energy function is defined such that the stress is determined from the gradient of the strain energy with respect to a strain tensor (for details see general texts on continuum mechanics and elasticity such as [9] and [10]). The strain energy function used for both the elasto-plastic and fictitious void materials is described by

$$W = \frac{1}{2}\kappa\left[p(J^{\frac{1}{p}} - 1) - \log(J)\right] + \frac{1}{2}\mu\left(\mathrm{tr}[\bar{\mathbf{B}}] - 3\right), \tag{3}$$

where the first part is due to the volumetric part of the deformation, and the second part is due to the distortional part of the deformation, J is the Jacobian of the deformation gradient which represents the volume change at a point, and $\bar{\mathbf{B}}$ is the deviatoric part of the left Cauchy Green tensor. In equation 3, p is a parameter which is introduced in order to increase the compressibility of the fictitious void material. Large values of p create a highly compressible material, where only small volumetric stresses are present under large volumetric deformations. This can be seen from figure 3 which shows the volumetric part of the strain energy for various values of p, where $J = 1$ corresponds to no volumetric change, therefore, a minimum in the strain energy. Notice that as p increases the strain energy becomes less sensitive to changes in volume until a certain point where the material stiffens rapidly. For these simulations, this behavior is critical for modeling the contact between the strands. For $p = \frac{1}{2}$ a realistic material is modeled which converges to Hooke's law for infinitesimal deformations. For this case, κ represents the bulk modulus and μ represents the shear modulus for an isotropic linear elastic material. A value of $p = \frac{1}{2}$ is used for the strand material in order to properly represent the elastic part of the elasto-plastic behavior.

For the fictitious void material, small values of κ and μ are used along with the previously described modified volumetric strain energy. It was found that using values of μ that are too small led to instabilities in the convergence of the solution due to the large amount of distortion of the fictitious void elements. However, if μ is too large, large deviatoric stresses build up in the void material which is undesirable. Therefore, values of μ that are large enough to avoid overly distorted elements are used, and the deviatoric part of the stress for the fictitious void elements is reset to zero at each step. This approach leads to stable convergence of the model while greatly limiting the magnitude of the deviatoric stress in the fictitious void material. It is

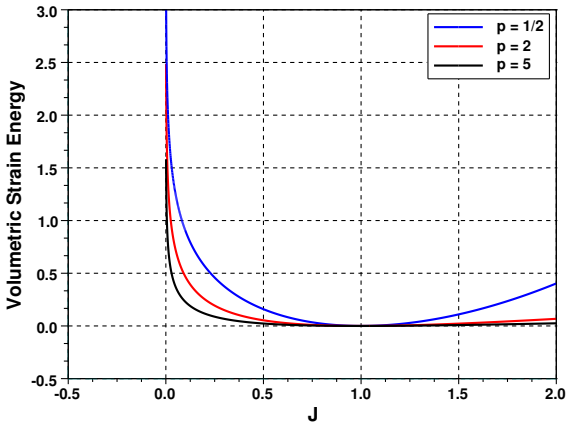

Figure 3. Volumetric strain energy as a function of the Jacobian of the deformation gradient. For larger values of p, the volumetric strain energy becomes less sensitive to volumetric changes until J approaches zero.

Table 1. Material properties for the strand and fictitious void materials used in the cable deformation example.

	κ (GPa)	μ (GPa)	p	A (MPa)	n	σ_y (MPa)
Strand	125.0	44.8	0.5	211.2	0.211	60.0
Void	10^{-2}	10^{-1}	8	-	-	-

reiterated here that these types of modifications to the material behavior can only be performed since the fictitious material is simply a modeling aid for these simulations and does not have to be representative of a real material.

2.3. Boundary conditions and solution

As mentioned earlier, the smallest possible unit cell is used for the cable deformation simulations. In order to obtain deformations compatible with "long" cables, periodic boundary conditions are implemented in the axial direction. The periodic boundary condition is described by

$$\mathbf{x}^+ - \mathbf{x}^- = \mathcal{F}(\mathbf{X}^+ - \mathbf{X}^-), \tag{4}$$

where $\mathbf{x}^+$ and $\mathbf{x}^-$ represent the positions of two points, in the deformed configuration, directly opposite to one another on the periodic surfaces, $\mathbf{X}^+$ and $\mathbf{X}^-$ are their corresponding positions in the undeformed configuration, and $\mathcal{F}$ is the average deformation gradient, which is a tensor that contains the ratio of the final to initial axial length of the unit cell. On the sides of the cable, the faces are assumed to compact in a frictionless manner; therefore, displacement boundary conditions are used where only the displacement degrees of freedom in the normal direction to the face are constrained. For a real cabling process, the final width and thickness of the cable can be readily obtained; however, the initial "undeformed" configuration is unknown since, for this case, it is simply a starting point for the model which is never built in an actual cabling process. Using only the usual cabling dimension information (width, thickness, strand diameter, number of strands, pitch length) there is no unique initial configuration. However, if the final packing factor is considered, a unique initial configuration can be found by determining the initial pitch angle that is necessary for the volume of the strands to be conserved. This configuration is then fully specified by the strand diameter, the number of strands, and the initial pitch angle. The boundary conditions that lead to the final deformed shape are selected by specifying the final width, thickness, and pitch for the cable.

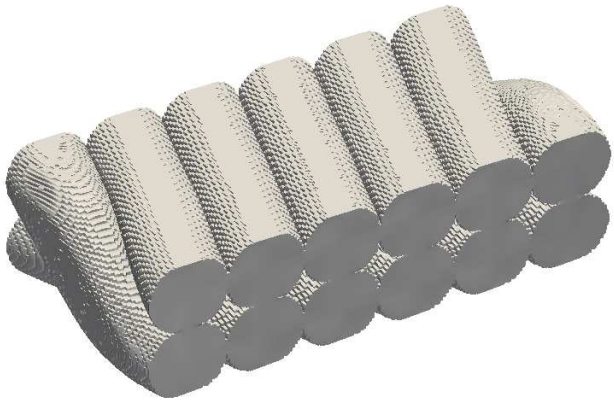

Figure 4. Final deformed configuration for a cable with an undeformed configuration that is shown in figure 2 and cabling parameters given in table 2.

Table 2. Parameter used in the cable deformation simulation.

N	d (mm)	ϕ_0	w (mm)	t (mm)	L_p (mm)
12	0.8	18.4°	5.25	1.42	30.4

For the implementation, the boundary conditions are applied using a penalty method. The non-linear system of equations is solved using the Newton-Raphson method with a line search. The line search proved to be critical for convergence the of this scheme. All of the code for the cable deformation simulation, as well as the subsequent simulations in this paper, is written Fortran.

2.4. Deformed cable example

In this section, an example of a cable deformation simulation is shown. This specific example consists of a mesh with 712 thousand elements and 2.2 million degrees of freedom. Table 2 shows the parameters that are used for this cable deformation example, where w is the final cable width, t is the final thickness, and L_p is the final pitch length, and as stated earlier, N is the number of strands, d is the diameter of the strands, and ϕ_0 is the initial pitch angle. As was previously described, the initial pitch angle is determined from the final cabling dimensions and the packing factor, which in this case is approximately 84%. Figure 4 shows the three-dimensional deformed shape of the cable. Figure 5 shows cross-sections of the cable at different points along the axis. These are compared to cross-sections taken from actual cables where the compaction parameters were attempted to be matched as well as possible. However, due to computational expense constraints, there is some ambiguity since the actual cable has 51 strands while the one used in the simulation has 12 strands. Qualitatively the simulation results match well with the real cable cross-sections; however, some differences are seen in the regions where two strands come together since the fictitious material elements can not completely collapse. Nevertheless, these elements seem to model the contact well since their volume can be substantially reduced, and the load is properly transferred with the stiffening of the elements under large volumetric changes.

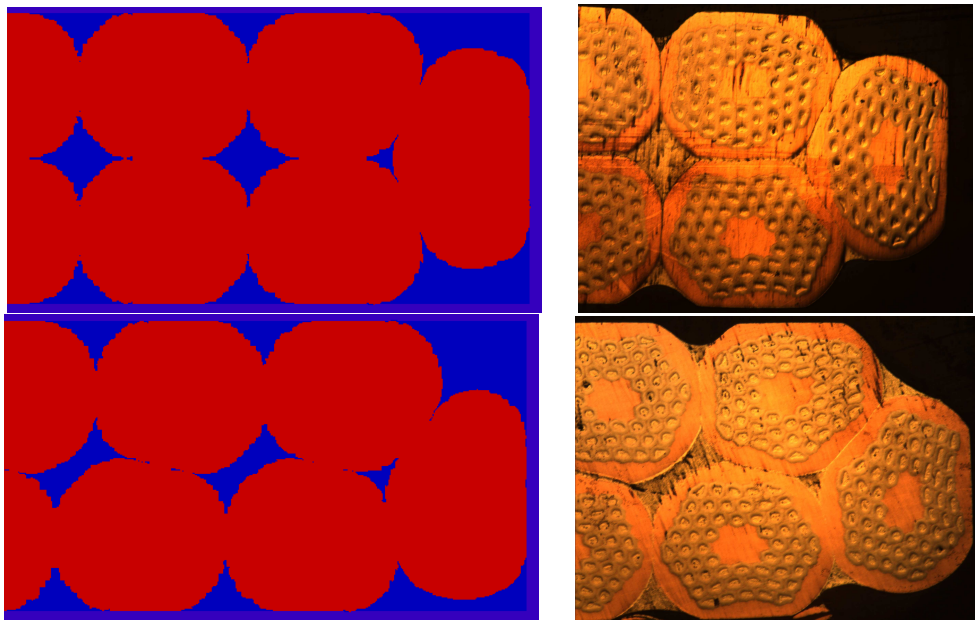

Figure 5. Comparison between cross-sections of the deformed cable from the simulation and a real cable for two different axial positions along the cable.

2.5. Determination of effective coil properties

Using the deformed cable model, the effective properties of a Rutherford cable "coil material" can be determined. In this case, the "coil material" is created by superimposing the unit cells in an infinite space. For a coil with a large number of cables, this is expected to be a reasonable approximation. In order to compute the effective properties, six different appropriate loading conditions can be applied to determine the effective elasticity tensor. Writing the stress strain linear elastic relation in engineering notation:

$$\begin{Bmatrix} \sigma_x \\ \sigma_y \\ \sigma_z \\ \tau_{xy} \\ \tau_{yz} \\ \tau_{zx} \end{Bmatrix} = \begin{bmatrix} C_{11} & C_{12} & C_{13} & C_{14} & C_{15} & C_{16} \\ C_{12} & C_{22} & C_{23} & C_{24} & C_{25} & C_{26} \\ C_{13} & C_{23} & C_{33} & C_{34} & C_{35} & C_{36} \\ C_{14} & C_{24} & C_{34} & C_{44} & C_{45} & C_{46} \\ C_{15} & C_{25} & C_{35} & C_{45} & C_{55} & C_{56} \\ C_{16} & C_{26} & C_{36} & C_{46} & C_{56} & C_{66} \end{bmatrix} \begin{Bmatrix} \varepsilon_x \\ \varepsilon_y \\ \varepsilon_z \\ \gamma_{xy} \\ \gamma_{yz} \\ \gamma_{zx} \end{Bmatrix} \tag{5}$$

it can be seen that if only one non-zero value of the strain components is chosen, then the corresponding column of the elasticity matrix can be determined by computing the stress tensor for that applied strain state. To extract the effective properties of the unit cell, six different average strain states over the defined domain are imposed, and the corresponding average stress states are calculated. For example, to compute the first column of the average elasticity matrix, a value of $\langle \varepsilon_x \rangle_\Omega$ is imposed with the other strain components set to zero and the average stress $\langle \boldsymbol{\sigma} \rangle_\Omega$ is computed. The operator $\langle \cdot \rangle_\Omega$ denotes the average over the domain Ω which corresponds to the unit cell. For more details on the extraction of effective properties and the choice of appropriate boundary conditions the interested reader is referred to the text by Zohdi and Wriggers [11]. For the case of periodic cells, the periodic boundary conditions that are given in equation 4 can be used. However, in this case, the boundary conditions are applied on all six faces of the unit cell since the material is assumed to be infinite in all directions.

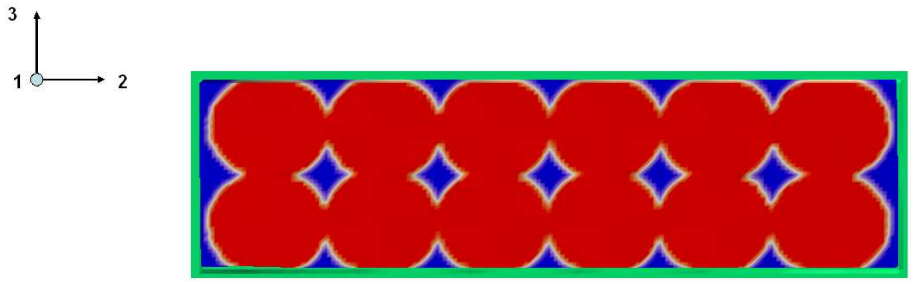

Figure 6. Cross-section of the unit cell used to determine the homogenized coil material. The green color represents the insulation layer, the blue represents the interstitial epoxy, and the red represents the strands.

As was the case with the cabling deformations, a regular hexahedral mesh is used with elements that are unaligned with the material interface and therefore contain multiple materials. For this model, over-integration is used in elements that contain multiple materials in order better capture the geometry inside of the element (see Zohdi [11] for details). Figure 6 shows an example of the cross-section of a unit cell which contains the deformed cable, the interstitial binder, and the outer insulation layer. In order to construct this model with a regular mesh, an intermediate mapping procedure is used to determine where the deformed cable material lies in the new mesh.

For the example considered here, the interstitial material is assumed to be epoxy with a Young's modulus of 5 GPa and Poisson's ratio of 0.3, the insulating layer is assumed to be an S-glass/epoxy composite with a 45/45 orientation. For the insulation, the material properties used are for a 60% volume fraction composite, which has a Young's modulus of 14.9 GPa along the direction of the cable axis and in the in-plane transverse direction, a Young's modulus of 6.7 GPa in the direction transverse to the plane, and shear moduli of 14.6 GPa and 4.82 GPa in and transverse to the plane respectively. Clearly, the accuracy of the individual material properties will have a large impact on the calculated homogenized properties. For the epoxy and insulation layers, reasonable values for the material properties are chosen; however, there is a fair amount of uncertainty in these values.

For this example, the strand properties are varied, where the highest value chosen is determined through a homogenization procedure of the macro-filament unit cell that is described below. This homogenization procedure leads to transversely isotropic properties with an axial Young's modulus of approximately 126 GPa where the Young's modulus of Nb_3Sn is taken to be 135 GPa at room temperature and that of Cu and bronze is taken to be 120 GPa. Using these individual properties, the homogenized properties turn out to be nearly isotropic; therefore, for simplicity, isotropic properties are used in the homogenization of the coil material. The value of the calculated Young's modulus for the strand may be higher than the apparent modulus for moderate strains due to the early onset of plasticity in the strands. For example, see [12] and [13] for data on mechanical measurements of superconducting strands. Therefore, the measured modulus in an experiment may be affected by lower apparent elasto-plastic modulus. Also, the stress strain curve for coil stacks can show highly non-linear behavior. This makes it difficult to obtain the elastic properties of the cable stack, although, as was shown in [14], a more linear behavior can be obtained by "massaging" the cable stack to a high enough load.

The calculated values for the orthotropic effective properties of the coil material at room temperature are shown in table 3 for three different values of the apparent Young's modulus of

Table 3. Calculated properties for the coil material which includes the cable, the interstitial epoxy, and the insulation layer. Results are presented for three different strand Young's moduli (E_s) and two different insulation thicknesses. The subscripts for the Young's moduli E, the Poisson's ratios ν, and the shear moduli μ correspond to the directions shown in figure 6, where 1 corresponds to the cable axis, 2 corresponds to the direction along the width of the cable, and 3 corresponds to the direction along the thickness of the cable.

	100 μm insulation			60 μm insulation		
E_s (GPa)	90	110	126	90	110	126
E_1 (GPa)	65.1	78.7	89.5	68.5	82.8	94.5
E_2 (GPa)	41.0	45.8	49.3	45.7	51.7	56.1
E_3 (GPa)	27.8	29.7	30.9	34.0	36.8	38.8
ν_{12}	0.34	0.34	0.34	0.34	0.34	0.34
ν_{23}	0.24	0.23	0.22	0.25	0.24	0.23
ν_{31}	0.14	0.12	0.11	0.16	0.14	0.13
μ_{12} (GPa)	19.4	22.0	23.8	20.5	23.5	25.7
μ_{23} (GPa)	13.7	14.9	15.6	15.2	16.8	17.8
μ_{31} (GPa)	14.8	16.1	17.0	16.8	18.8	20.2

the strand (E_s) and two different insulation thicknesses. The subscripts for the Young's moduli E, the Poisson's ratios ν, and the shear moduli μ in table 3 correspond to the directions shown in figure 6, where 1 corresponds to the cable axis, 2 corresponds to the direction along the width of the cable, and 3 corresponds to the direction along the thickness of the cable. For the Poisson's ratios, ν_{ij} are defined as the negative of the transverse strain in the j-direction over the strain in the i-direction, when stress is applied only in the i-direction. The remaining Poisson's ratios can be found using the relation

$$\nu_{ji} = \nu_{ij} \frac{E_j}{E_i}. \tag{6}$$

As can be seen from table 3 the Young's modulus in the 3 direction is highly sensitive to the thickness of the insulation layer. This also suggests that it is highly sensitive to the material properties of the insulation layer. This is expected since the ratio of the amount of insulation to cable is highest in this direction. The Young's modulus in the 1 direction is seen to be more sensitive to the properties of the strand material. The values for the Young's modulus at room temperature in the 3 direction seem to be in reasonable agreement with the experimental data reported in [14], where values of 18 GPa and 39 GPa are given for monotonic loading and after initial loading to 100 MPa respectively.

3. Unit cell model of RRP strand macro-filament

In order to obtain the homogeneous properties of the strands and to determine the local fields from the larger scale homogenized strand/cable solution, a unit cell model of RRP macro-filaments is developed. Figure 7 shows the unit cell used for this model which is a periodic structure containing a total of two filaments and the interstitial matrix material. For this case, only linear elastic properties are considered and the materials are assumed to be bronze, Cu, and Nb_3Sn. In order to obtain the effective properties of the superconducting region of the strand (the region containing the subelements) the same homogenization technique that was described in the previous section for the coil material is used. This leads to a value of 126 GPa for a

strand with 40% Nb_3Sn, where the Young's modulus of Nb_3Sn is taken to be 135 GPa (see [1] for various temperature dependent material properties), and the modulus of Cu and bronze is 120 GPa. In order to determine the localized behavior in the unit cell, an average strain over the unit cell is applied through the boundary conditions, and the localized stress and strain fields are solved.

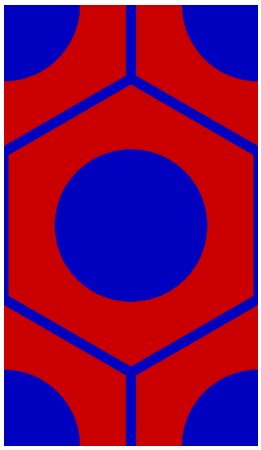

Figure 7. Unit cell for RRP strand macro-filaments. The red area represents the Nb_3Sn region, while the blue represents Cu and bronze regions.

4. Multi-scale coupling

In this work, a simplified framework is used where only the linear elastic case is considered for the multi-scale coupling. Since the material behavior is linear, the material properties are constants that are independent of the deformation. This leads to a trivial coupling procedure where the strain state at a localized region in a larger-scale problem is simply transferred as the average strain state over a unit cell at the smaller scale. This type of coupling is considered reasonable if the gradient of the strain fields are fairly homogeneous over a large enough region. This is expected to be the case in coupling the coil length scale to the cable length scale and also in the coupling between the cable length scale and the strand/macro-filament length scale. For the cable length scale, this is true since the strain is fairly homogeneous over the homogenized strand cross-section due to the flattening of the cable and the interstitial epoxy which smooths the strain fields. However, since the unit cell is in an undeformed configuration, this may lead to errors in the localized stress and strain state. Nevertheless, it serves as an initial approximation and may be useful for cases where the subelements are not highly deformed.

5. Conclusions

This work presents part of an overall goal, which is continuing to develop realistic three-dimensional simulations to determine the strain state inside the superconducting filaments. The development of the cabling simulation is an important step in obtaining realistic three-dimensional models of the deformed strands; however, at this time the strands do not include the subelements. Since the deformed three-dimensional subelement shapes are unknown at this time, the macro-filament unit cell model includes undeformed sub-elements. Determining the deformed shapes of the subelements in three-dimensional setting will be critical to obtaining the real strain state in these filaments. In the work presented here, only elastic deformations are included for the hierarchical component of the simulations. This is done as a first step since the homogenized properties are independent of deformation; therefore, an iterative solution process that can be expensive is not necessary. Furthermore, this iteration may need to be performed at every integration point in the finite element model which can quickly become an intractable problem. At LBNL, work is ongoing in developing simplified non-linear hierarchical models that

include the non-linear material effects, but at a lower computational expense. In summary, the work presented here is an important step, mainly in the calculation of the three dimensional deformation of the cables, in a larger framework to bridge the multiple scales while including the relevant physical behaviors. The deformed cable geometry is critical in obtaining the initial configuration for the hierarchical simulations of magnets that are fabricated with Rutherford cables.

Acknowledgments
The authors would like to acknowledge Marco La China for obtaining a solution to the initial cable geometry with the intersecting cylinder model. This work was supported by the Director, Office of Science, High Energy Physics, U.S. Department of Energy, under contract No. (DE-AC02-05CH11231).

References

[1] Mitchell N 2005 *Cryogenics* **45** 501
[2] Mitchell N 2005 *IEEE Trans. Appl. Supercond.* **15** 3572
[3] Ahoranta M, Lehtonen J, Tarhasaari T and Weiss K 2008 *Supercond. Sci. Technol.* **21** 025005
[4] Boso D, Lefik M and Schrefler B 2005 *Cryogenics* **45** 259
[5] Boso D, Lefik M and Schrefler B 2005 *Cryogenics* **45** 589
[6] Farinon S, Boutboul T, Devred A, Leroy D and Oberli L 2007 *IEEE Trans. Appl. Supercond.* **17** 1136
[7] Farinon S, Boutboul T, Devred A, Leroy D and Oberli L 2008 *IEEE Trans. Appl. Supercond.* **18** 984
[8] Simo J 1988 *Comput. Meths. Appl. Mech. Engrg.* **68** 1
[9] Gurtin M 2003 *An Introduction to Continuum Mechanics (Mathematics in Science and Engineering)* (Elsevier Science (USA))
[10] Ogden R 1984 *Non-Linear Elastic Deformations* (Dover)
[11] Zohdi T and Wriggers P 2005 *An Introduction to Computational Micromechanics* (Springer-Verlag)
[12] van den Eijnden N, Nijhuis A, Ilyin Y, Wessel W and ten Kate H 2005 *Supercond. Sci. Technol.* **18** 1523
[13] Nyilas A 2005 *Supercond. Sci. Technol.* **18** S409
[14] Chichili D, Arkan T, Ozelis J and Terechkine I 2000 *IEEE Trans. Appl. Supercond.* **10**